



# Spermiogenesis of the hangingfly *Terrobittacus implicatus* (Huang and Hua) (Mecoptera: Bittacidae)

Ying Miao<sup>1</sup> · Bing-Peng Liu<sup>1</sup> · Bao-Zhen Hua<sup>1</sup>

Received: 4 April 2019 / Accepted: 4 July 2019 / Published online: 10 July 2019  
© Springer-Verlag GmbH Austria, part of Springer Nature 2019

## Abstract

The structure of spermatozoa is able to provide valuable characters in resolving phylogenetic relationships in Metazoa, especially in insects. Such data, however, are greatly deficient in Mecoptera. Here, we studied the spermiogenesis and ultrastructure of sperm in the hangingfly *Terrobittacus implicatus* (Huang and Hua) using transmission electron microscopy. The results show that the spermatogenesis of *T. implicatus* occurs within sperm cysts, following a pattern commonly found in insects. The microtubular doublets of spermatid axoneme exhibit a hooklike projection from the B-subtubule in the early period, but the projection disappears in the mature stage. The mature spermatozoon of *T. implicatus* is a filiform cell that is pronouncedly elongated and has a bi-layered acrosome, a nucleus with two lateral longitudinal grooves, a neck region with the centriole adjunct, a flagellum with a simple 9 + 2 axoneme, two extra-axonemal accessory structures, two accessory bodies, and two mitochondrial derivatives of unequal size, and a prominent glycocalyx. The basic structure of spermatozoa of *T. implicatus* is similar to that of other Mecoptera studied. However, this species shows characteristics unique in Bittacidae, such as the reniform appearance of the centriole adjunct, two triangular accessory bodies with granular materials, and two asymmetric mitochondrial derivatives with a circular profile in cross-section. The potential utilization of the sperm ultrastructure for understanding the phylogeny of Bittacidae is briefly discussed.

**Keywords** Sperm · Centriole adjunct · Accessory body · *Terrobittacus* · Phylogeny

## Introduction

Spermiogenesis is a differentiation process of post-meiotic male germ cells (spermatids) into mature spermatozoa (Nantel et al. 1996; Chapman 2013). Owing to the rapid evolutionary divergence (Baccetti 1972, 1998; Dallai et al. 2006; Dallai 2014), the sperm characters are important resources for resolving taxonomic and phylogenetic issues in insects (Jamieson et al. 1999; Dallai et al. 2011a, 2016a; Gottardo et al. 2016). A vast number of investigations have been reported on the morphology of mature sperm in Insecta (Jamieson et al. 1999; Dallai et al. 2006, 2016a, b, 2019; Nardi et al. 2013; Dallai 2014; Gottardo et al. 2016; Cuquetto-Leite

et al. 2017; Zhang and Hua 2017; Santos and Lino-Neto 2018), but only a few involved spermiogenesis, especially in Mecoptera.

Bittacidae is the second largest family in Mecoptera and currently consists of 18 genera worldwide (Chen et al. 2013). The adults of Bittacidae are commonly known as hangingflies because they are unable to stand on a surface but suspend themselves from the edges of leaves or twigs using the prehensile tarsus between flights (Bornemissza 1966; Byers and Thornhill 1983; Penny 2006; Tan and Hua 2008). Owing to the specialized morphology, the phylogenetic position of Bittacidae remains unsatisfactorily resolved in Mecoptera. Based on morphological phylogeny, Bittacidae was regarded as a basal-most taxon in extant Pistillifera next to Nannochoristidae (Willmann 1987, 1989). The molecular evidence, however, indicates that Bittacidae and Panorpididae form a clade as the sister group to Panorpidae (Whiting 2002). From the head structures, Bittacidae has a sister relationship with the group consisting of Apteropanorpidae, Choristidae, Eomeropidae, Panorpidae, and Panorpididae (Beutel and Baum 2008; Friedrich et al. 2013).

Handling Editor: Georg Krohne

✉ Bao-Zhen Hua  
huabzh@nwfufu.edu.cn

<sup>1</sup> Key Laboratory of Plant Protection Resources and Pest Management, Ministry of Education, College of Plant Protection, Northwest A&F University, Yangling 712100, Shaanxi, China

The sperm data are considerably scarce in Bittacidae so far. Shepardson et al. (2014) provided the only investigation of sperm ultrastructure for two *Bittacus* species and described a unique phenomenon that one mitochondrial derivative was displaced by an accessory body. The low quality of their figures, however, made the results less convincing. Moreover, the spermiogenesis process remains unknown in Bittacidae.

In this study, we investigated the spermiogenesis and sperm ultrastructure of *Terrobittacus implicatus* (Huang and Hua in Cai et al. 2006) (Tan and Hua 2009) using transmission electron microscopy, in the attempt to add new information of spermiogenesis in Bittacidae and to contribute to the identification of new sperm ultrastructural characters for future phylogenetic analyses of Mecoptera.

## Materials and methods

### Biological materials

Adults of *T. implicatus* were collected from the Huoditang Forest Farm (33° 26' N, 108° 26' E, elev. 1600–1800 m) in the Qinling Mountains, Shaanxi Province, central China, in early August from 2016 to 2017.

### Insect rearing

Live adults were reared in screen-wired cages (40 cm × 60 cm × 60 cm) containing twigs and leaves of plants and moist absorbent cotton following Miao and Hua (2017). The eggs, larvae, and pupae were incubated and reared in plastic containers with humid humus. Live flies and frozen pupae (*Musca domestica*) were provided as food items for the adults and larvae, respectively. The eggs, larvae, and pupae were reared in the laboratory from September 2016 to May 2017. The temperature was kept at 16 ± 2 °C for the larvae, 21 ± 2 °C for the pupae, and 23 ± 2 °C for the adults. The relative humidity was 75 ± 10%.

### Transmission electron microscopy

The testes of fourth-instar larvae, pupae, and newly emerged adults were dissected out rapidly and immediately fixed in a mixture of 2.0% paraformaldehyde and 2.5% glutaraldehyde in 0.1 M phosphate buffer (PB, pH 7.2) at 4 °C for 6 h (Karnovsky 1964; Zhang et al. 2017). The fixed samples were rinsed with PB, and post-fixed with 1% osmium tetroxide (OSO<sub>4</sub>) at 4 °C for 1.5 h. The testes were dehydrated through a graded series of acetone (30%, 50%, 70%, 80%, 90%, and 100%) and infiltrated successively through three mixtures of acetone/Epon 812 resin (3:1, 1:1, and 1:3) and pure Epon 812 resin at room temperature. The dehydrated samples were embedded in pure Epon 812 resin, polymerized at 30 °C for 24 h

and 60 °C for 48 h. The resin-embedded testes were cut into 50-nm-thick sections using a diamond knife on a Leica EM UC7 ultramicrotome (Leica, Nussloch, Germany). Ultrathin sections were double stained with uranyl acetate and lead citrate for 10 and 8 min, respectively, and then examined under a Tecnai G2 Spirit Bio Twin transmission electron microscope (FEI, Hillsboro, USA).

## Results

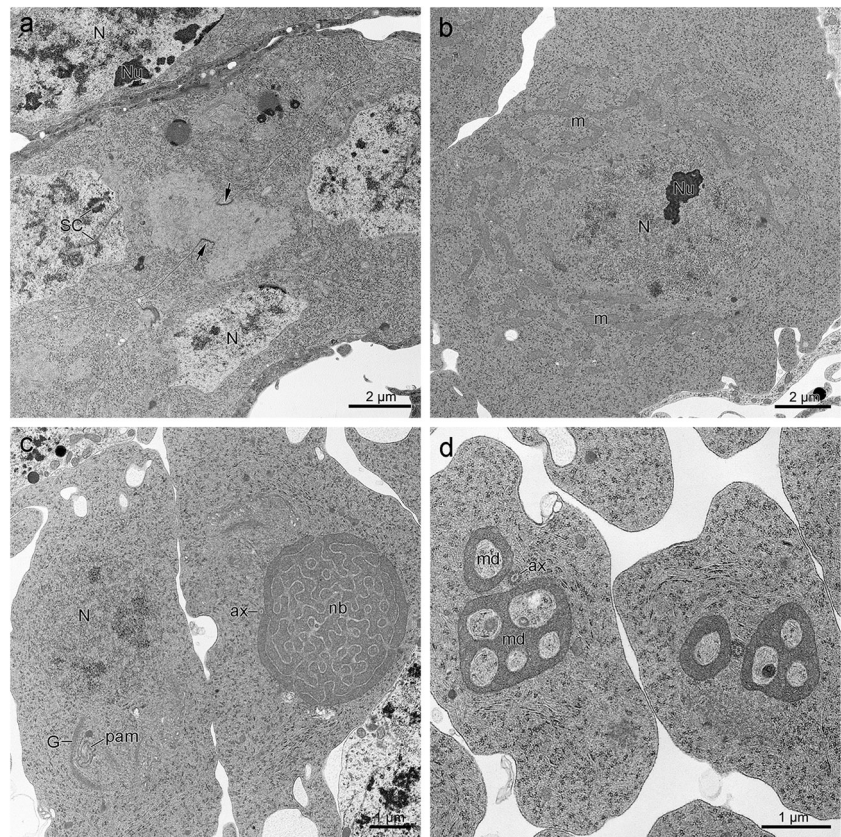
### Spermiogenesis

Primary spermatocytes are formed after spermatogonial divisions. They are connected to each other by cytoplasmic bridges and are recognized by the nucleus with diffuse chromatin and evident synaptonemal complexes (Fig. 1a). During the meiotic division, a large number of scattered mitochondria are visible in the cytoplasm (Fig. 1b). The early spermatids are characterized by a spherical nucleus with dispersed chromatin, a large “nebenkern”, and a conspicuous Golgi system with the pro-acrosome material presented in the fossa of the Golgi apparatus (Fig. 1c). The nebenkern is then divided into two halves (mitochondrial derivatives) of unequal size and lies parallel on both sides of the incipient axoneme (Fig. 1d). Each half contains many irregularly oriented cristae and several large vacuoles.

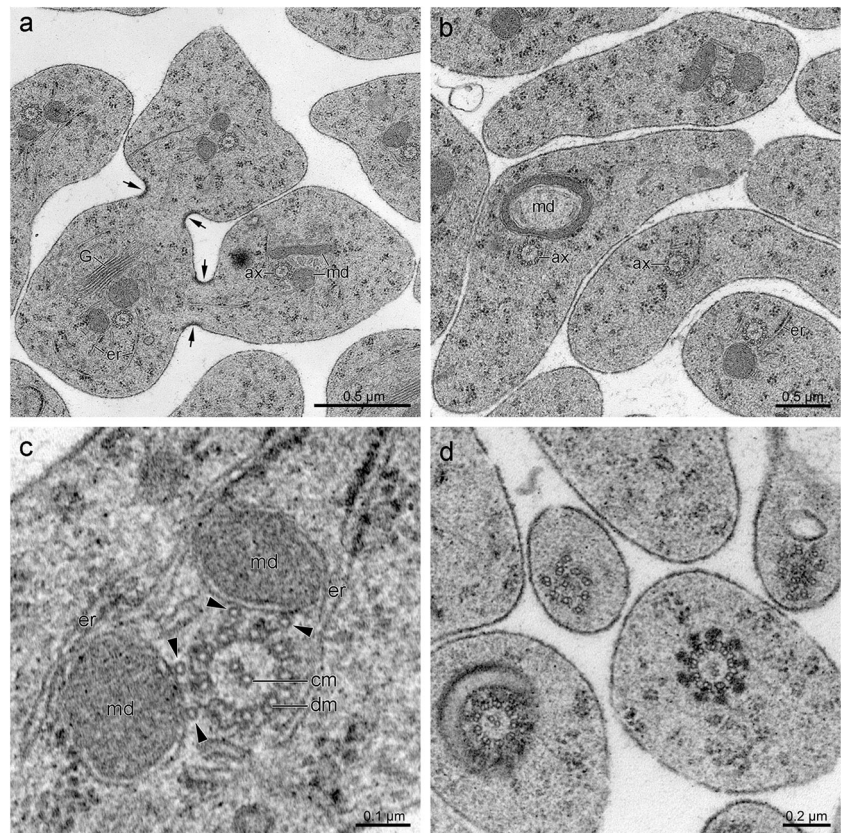
At the early stage of spermiogenesis, spermatids are interconnected by cytoplasmic bridges and exhibit large amount of cytoplasm (Fig. 2a). The cross-section of the flagellar region shows that one mitochondrial derivative terminates before the other (Fig. 2b). The axoneme has a simple 9 + 2 pattern with two central microtubules and nine doublets (Fig. 2c). Up to four cytoplasmic microtubules are observed outside the axoneme. At the posterior extremity of the flagellum, the axoneme loses its regular configuration (Fig. 2d). An interesting cross-section of the axoneme is visible at the same level. The axoneme on the right side shows nine dense amounts of material outside the 9 + 2 (Fig. 2d).

The spermiogenesis proceeds with the elongation of the spermatid components. The bell-shaped acrosome arising from the Golgi complex is visible on the top of the elliptical nucleus (Fig. 3a). This structure shows a compact dense region, corresponding to the acrosome vesicle. The sub-acrosomal space is represented by a longitudinal canal, within which filamentous material is visible (Fig. 3a, arrow). This material is the early perforatorium. Beneath the nucleus, the anterior portion of axoneme inserts into one side of the posterior extremity of the nucleus and it is surrounded by the centriole adjunct, which is well developed and is shown as a dense layer (Fig. 3b, c). In the flagellar region, the endoplasmic reticulum runs along the axoneme and mitochondrial derivatives (Fig. 3d). The axoneme exhibits a 9 + 2 pattern with

**Fig. 1** Spermatocytes and early spermatids of *Terrobittacus implicatus*. **a** Primary spermatocytes at meiotic prophase, showing that the cells are interconnected by a cytoplasmic bridge (arrows). The nucleus is characterized by the synaptonemal complexes. **b** Spermatocytes after division processes with large number of scattered mitochondria in the cytoplasm. **c** Early spermatids characterized by dispersed chromatin in the nucleus and by the presence of a prominent “nebenkern,” the Golgi apparatus, and the pro-acrosome material. **d** Spermatids with the nebenkern divided into two mitochondrial derivatives along the two sides of axoneme. ax axoneme, G Golgi apparatus, m mitochondria, md mitochondrial derivative, nb nebenkern, N nucleus, Nu nucleolus, pam pro-acrosome material, SC synaptonemal complex



**Fig. 2** Cross-sections through the flagellar region of maturing spermatids of *Terrobittacus implicatus*. **a** Three spermatids interconnected by cytoplasmic bridges. Arrows point to the cytoplasmic bridges with evident densities at the opposite sides. **b** Different levels of the flagellar region, showing that mitochondrial derivatives progressively diminished until only the axoneme left. **c** Details of the spermatid axoneme with nine doublets, two central microtubules, and four cytoplasmic microtubules (arrowheads) positioned outside the nine axonemal doublets. **d** Cross-section through the flagellar posterior tip, showing the axoneme disorganization. ax axoneme, cm central microtubule, dm doublet, er endoplasmic reticulum, G Golgi apparatus, md mitochondrial derivative



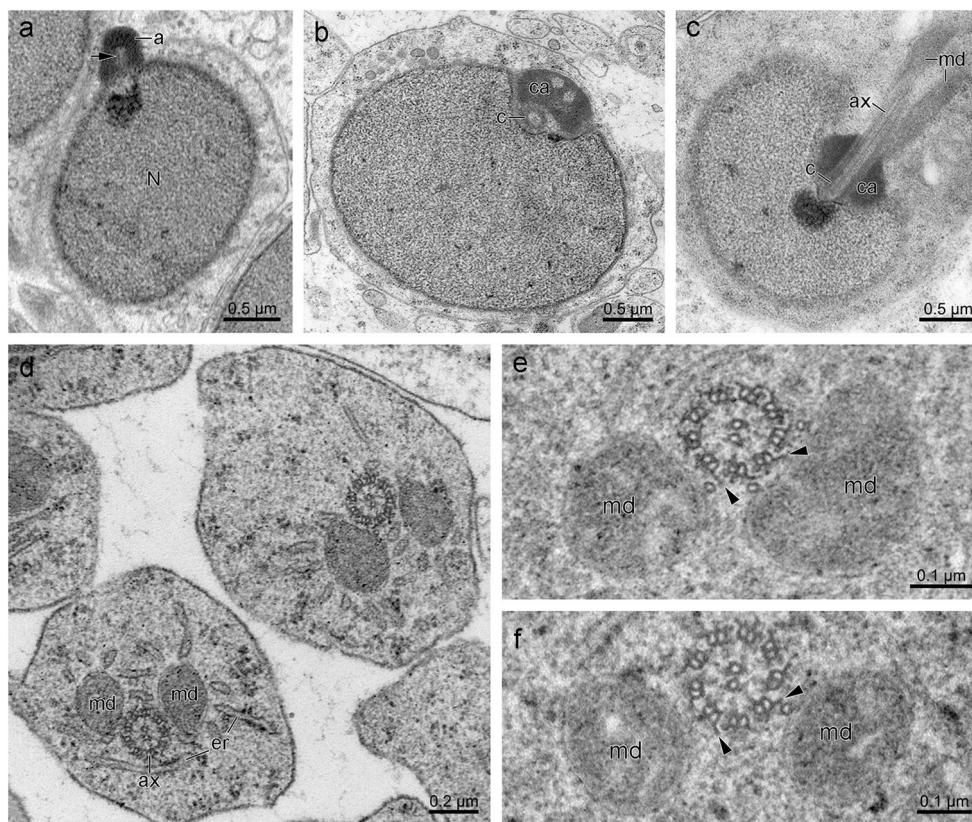


**Fig. 3** Elongating spermatids of *Terrobitacus implicatus*. **a** Longitudinal section through the roundish homogeneously dense nucleus with a bell-shaped acrosome on the top. At half-length of the acrosome, the inner perforatorium (arrow) space is visible. **b** Cross-section through the centriolar region beneath the spermatid nucleus, showing the centriole and the sheath-like centriole adjunct. **c** Longitudinal section through the anterior region of a spermatid, showing the centriole surrounded by the dense centriole adjunct, the flagellar axoneme, and two mitochondrial

derivatives. **d** Cross-section through the flagellum, showing the axoneme, endoplasmic reticulum, and two mitochondrial derivatives. **e, f** The flagellar axoneme shows a 9 + 2 microtubular pattern: two central microtubules, and nine microtubular doublets with dynein arms and a backward-oriented projection (arrowheads). a acrosome, ax axoneme, c centriole, ca centriole adjunct, er endoplasmic reticulum, md mitochondrial derivative, N nucleus

nine doublet microtubules and two central microtubules (Fig. 3d–f). The microtubular doublets of the flagellar axoneme exhibit a backward-oriented projection from the B-subtubule (Fig. 3e, f), reminiscent of the forming accessory tubule. This projection points in a direction opposite to that of the dynein arms. Occasionally, a few cytoplasmic microtubules can be observed outside the axonemal doublets (Fig. 3e, f).

During late spermiogenesis, the spermatids undergo evident modifications. The chromatin in the nucleus is transformed from a dispersed to a granular state and subsequently coalesces to dense masses (Fig. 4a). The centriolar region is well developed and surrounded by the centriole adjunct, which is found to assemble in the concave part of the nucleus (Fig. 4a, b). The centriole adjunct forms a compact sleeve, encircling the anterior region of the axoneme and one mitochondrial derivative (Fig. 4b). In the flagellum, a process of crystallization starts in the mitochondrial derivatives with dense materials deposited on the inner mitochondrial membrane on the side facing the axoneme (Fig. 4c). The axonemal doublets have no extensions from the B-subtubule at maturity

(Fig. 4d). The accessory bodies are formed between the axoneme and the flattened Golgi-derived cistern during this stage (Fig. 4d).

### Ultrastructure of the spermatozoa

The spermatozoon of *T. implicatus* is a filiform cell approximately 2000  $\mu\text{m}$  in length (Fig. 5a) and consists of a short head, a neck transition region, and a long posterior flagellum (Fig. 5).

The head, measuring approximately 36.5- $\mu\text{m}$  long (Fig. 5a, inset), is composed of a bi-layered acrosome (approximately 1.5- $\mu\text{m}$  long) and an elongate nucleus with very homogeneously compact chromatin (Fig. 5b, d). It is generally cylindrical, but has two shallow grooves. In the lateral grooves, some filiform materials are present (Fig. 5d).

The neck transition region is composed of the centriole adjunct, the basal body anchored to the nucleus, and the anterior portions of the axoneme. The centriole adjunct is electron-dense and located beneath the nucleus. In cross-

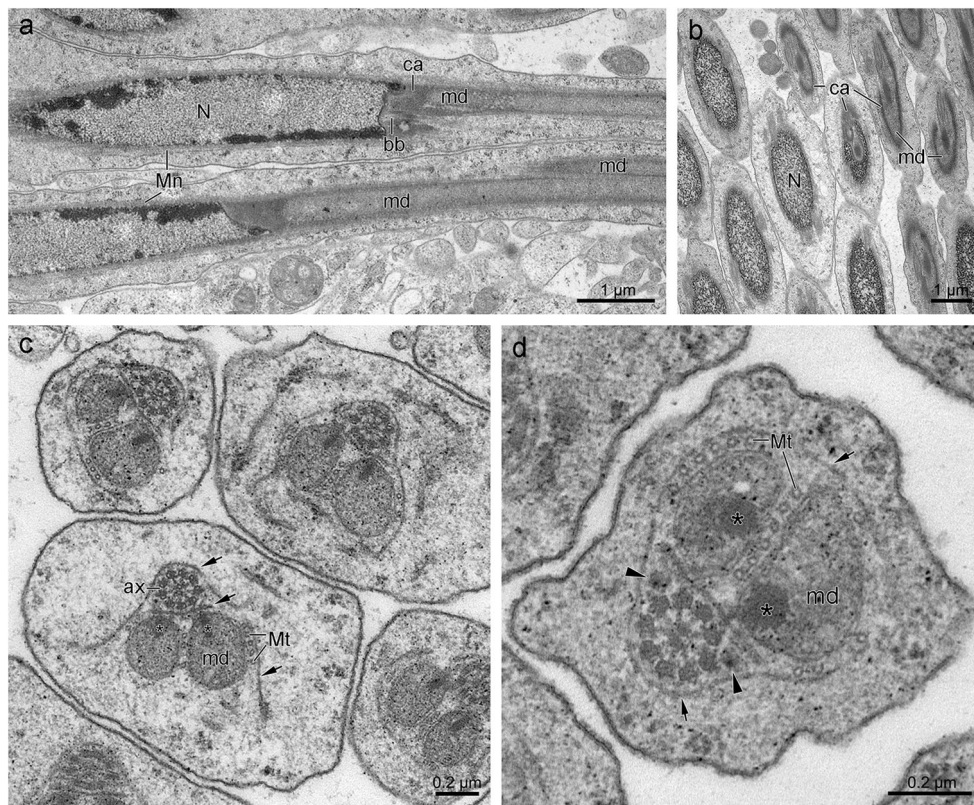


**Fig. 4** Late spermatids of *Terrobittacus implicatus* in longitudinal (**a**) and cross (**b–d**) sections. **a** The anterior region of a spermatid, showing the elongating nucleus, the basal body, the centriole adjunct, and the mitochondrial derivatives. **b** A sperm cyst at the neck-transition level. The centriole adjunct, appearing as a compact sleeve, encircles the anterior portion of axoneme and one mitochondrial derivative. **c** The flagellum of an aged spermatid, showing that both mitochondrial derivatives have a small region of electron-dense crystalline materials (asterisks), which deposit on the inner mitochondrial membrane on the side facing

the axoneme. A system of Golgi complex-derived membranous cisterns (arrows) begin to surround the mitochondrial derivatives and the axoneme. **d** The flagellum of an almost mature spermatid. The paired accessory bodies (arrowheads) are visible between the axoneme and both mitochondrial derivatives with large region of crystalline materials (asterisks). A system of Golgi complex-derived membranous cisterns (arrows) surround the flagellar components, forming the definitive spermatozoon plasma membrane. ax axoneme, bb basal body, ca centriole adjunct, md mitochondrial derivative, Mn manchette, Mt microtubule, N nucleus

section, the centriole adjunct displays a reniform appearance parallel to the axoneme (Fig. 5e). The axoneme exhibits a 9 + 2 pattern: nine doublet microtubules with dynein arms and thick radial spokes, and two central microtubules (Fig. 5e, f).

The flagellum is helical along its entire length (Fig. 5c) and has an axoneme, two mitochondrial derivatives, two accessory bodies, and two extra-axonemal dense rods (Fig. 5f). The two mitochondrial derivatives occur at different levels and differ in length and diameter. Both mitochondrial derivatives display a large crystalline organization and a circular shape in cross-sections. The accessory bodies are almost triangular in cross-sections, situated between the axoneme and mitochondrial derivatives. The two extra rods are electron-dense and dot-shaped (20-nm thick) in cross-section, situated between the axoneme and mitochondrial derivatives along the flagellum (Fig. 5e).

At maturity, the plasma membrane of sperm is covered by a dense layer of glycocalyx 25-nm thick (Fig. 5b–f).

## Discussion

The present study may represent the first attempt to investigate the spermiogenesis and sperm ultrastructure of *T. implicatus*, a member of the family Bittacidae whose data on male gametogenesis are very scarce in the literature.

The spermiogenesis of *T. implicatus* occurs within sperm cysts, following a pattern commonly found in insects (Phillips 1970; Jamieson et al. 1999; Dallai 2014; Dias et al. 2015; Novais et al. 2017). The number of spermatids per cyst is  $2^7 = 128$ , same with the observation in *Bittacus* (Shepardson et al. 2014). Early spermatids develop a conspicuous “nebenkern”, which is further divided into two mitochondrial derivatives of unequal size. The bi-layered acrosome is formed by a large Golgi complex, as is found commonly in Dicondylia (Jamieson et al. 1999; Dallai et al. 2011b; Dallai 2014; Gottardo et al. 2016; Zhang and Hua 2017). The terminal differentiation of spermatids proceeds as usual among mecopterans involving the microtubular “manchette”

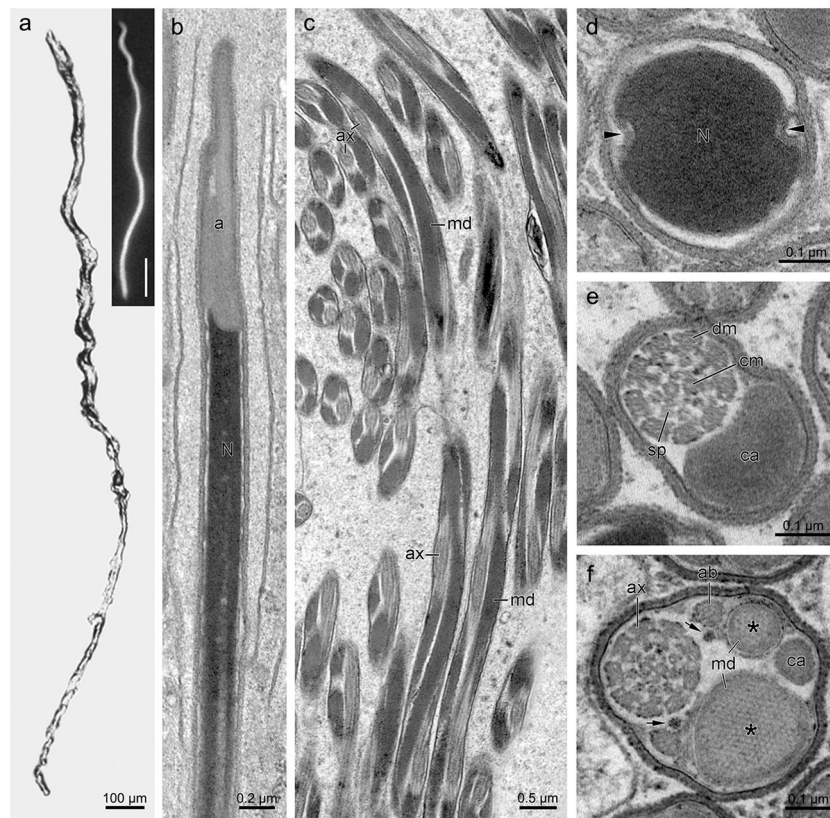


**Fig. 5** The mature spermatozoa of *Terrobittacus implicatus* under light (a) and electron microscopy (b–f). **a** Phase contrast micrograph of a sperm bundle. Inset shows the magnification of the head region stained with DAPI, and the scale bar is 5 µm. **b** The head region of a spermatozoon, showing the short acrosome and the cylindrical nucleus. **c** The flagellar region, showing the helicoidal array of mitochondrial derivatives and the axoneme. **d** The nucleus with filiform materials (arrowheads) alongside the two lateral grooves. **e** The neck-transition

region, showing the reniform centriole adjunct and the 9 + 2 axoneme. **f** The basal part of the flagellum, consisting of the axoneme, the centriole adjunct, two extra-axonemal dense rods (arrows), two triangular accessory bodies, and two unequal mitochondrial derivatives with inner crystalline materials (asterisks). a acrosome, ab accessory body, ax axoneme, ca centriole adjunct, cm central microtubule, dm doublet, md mitochondrial derivative, N nucleus, sp spoke

surrounding the sperm components (Dallai et al. 2003; Shepardson et al. 2014; Zhang et al. 2017).

The axonemal doublets of the spermatid flagellum have a backward-oriented projection in the early spermiogenesis of *T. implicatus*. The structure is similar to that described for the fruit fly *Drosophila melanogaster* Meigen (Gottardo et al. 2018) and the silverfish *Tricholepidion gertschi* Wygodzinsky (Dallai et al. 2001), resembling the first stage in forming the accessory tubule of Dicondylia (Dallai and Afzelius 1990; Dallai et al. 2006; Dallai 2014). Moreover, nine dense bodies were observed to be present on the outer side of doublets during the spermiogenesis (Fig. 2d). Such dense material is similar to the intertubular material, which is associated with the accessory tubules and only positioned outside the doublets of the 9 + 9 + 2 axoneme (Dallai et al. 2001, 2006; Zizzari et al. 2008; Gottardo et al. 2012, 2018; Dallai 2014). The present data imply that the accessory tubules are secondarily lost in the sperm of *Terrobittacus* species and may provide additional supports for the reversal origin of the 9 + 2 flagellar axoneme in Mecoptera (Dallai 1979, 2014; Dallai et al. 2003, 2016a; Zhang and Hua 2014).

The spermatozoa of *T. implicatus* are elongated filiform cells, and share the sperm characteristics with other mecopterans as follows: a bi-layered acrosome, a nucleus with two lateral longitudinal grooves, a neck-transition region with the centriole adjunct, a flagellum with a simple 9 + 2 axoneme, two extra-axonemal dense rods and two mitochondrial derivatives, and a prominent glycocalyx (Breland et al. 1966; Baccetti 1972; Gassner et al. 1972; Jamieson et al. 1999; Dallai et al. 2003; Russell et al. 2013; Shepardson et al. 2014; Zhang and Hua 2014, 2017; Zhang et al. 2016, 2017). However, the *Terrobittacus* sperm exhibit some peculiar features: (1) the centriole adjunct with a reniform transection, (2) the occurrence of two triangular accessory bodies with granular materials, and (3) two asymmetric mitochondrial derivatives with a circular profile in cross-section.

An uncommon feature of sperm in Mecoptera is the presence of two small extra-axonemal dense rods near the two accessory bodies. The presence of such structures in Panorpididae, Panorpididae, Boreidae, and Bittacididae represents a striking synapomorphy uniting these taxa (Breland et al. 1966; Dallai et al. 2003; Russell et al.

2013; Shepardson et al. 2014; Zhang and Hua 2014, 2017; Zhang et al. 2016, 2017).

The notable feature of *Terrobittacus* spermatozoa lies in the neck-transition region, which is the location of the centriole adjunct. In *T. implicatus*, as occurs in the spermatozoa of *Bittacus* (Shepardson et al. 2014), the centriole adjunct extends parallel to the basal part of the axoneme and the two mitochondrial derivatives. On the contrary, the centriole adjunct surrounds both the centriole and the proximal part of two mitochondrial derivatives in Panorpidae (Dallai et al. 2003) or embraces the centriole, and one of the two mitochondrial derivatives in Panorpididae (Zhang and Hua 2014) and Boreidae (Dallai et al. 2003; Russell et al. 2013).

It is worth noting that Shepardson et al. (2014) seemed to confuse the centriole adjunct with the accessory body. The centriole adjunct and the accessory bodies are related structures involved in insect sperm development (Dallai et al. 2016b). The former is an electron-dense material and appears in the early spermiogenesis, surrounding the centriole and the later basal body (Breland et al. 1966; Baccetti 1972; Jamieson et al. 1999; Dallai 2014; Dallai et al. 2016a, b), whereas the latter is likely to originate from the centriole adjunct, and normally interposed between the axoneme and the mitochondrial derivatives (Gottardo et al. 2012; Dallai et al. 2016a, b). Based on our observations, the centriole adjunct occurs in the early spermatids (Fig. 3b, c), but the accessory bodies appear later, after the crystallization of mitochondrial derivatives (Fig. 4c, d). In the mature sperm of *T. implicatus*, the centriole adjunct beneath the nucleus exhibits an electron-dense appearance and extends laterally to the mitochondrial derivatives with an almost triangular transection (Fig. 5e), similar to the descriptions of the accessory body by Shepardson et al. (2014). This evidence indicates that the sole accessory body found in *Bittacus* is probably the centriole adjunct.

The accessory body is the typical component of the mecopteran spermatozoa (Gassner et al. 1972; Dallai et al. 2003; Russell et al. 2013; Zhang and Hua 2014, 2017; Zhang et al. 2016, 2017). It is always present between the axoneme and the two mitochondrial derivatives, but varies in number and appearance. The spermatozoa of *T. implicatus* are characterized by the presence of two distinct accessory bodies consisting of the granular material. Two accessory bodies are also present in the spermatozoa of Boreidae (Dallai et al. 2003; Russell et al. 2013), Panorpididae (Zhang and Hua 2014) and *Panorpa liui* Hua of Panorpidae (Zhang et al. 2017). Because most species of Panorpidae studied have only one diffused accessory body (Gassner et al. 1972; Dallai et al. 2003; Zhang et al. 2016; Zhang and Hua 2017), we propose that the number of the accessory body are unsuitable for phylogenetic analyses in Mecoptera.

*Terrobittacus implicatus* has two asymmetric mitochondrial derivatives with pronounced differences in length and diameter, as in almost all the other species studied previously in

Mecoptera (Breland et al. 1966; Baccetti 1972; Gassner et al. 1972; Jamieson et al. 1999; Shepardson et al. 2014; Zhang and Hua 2014, 2017; Zhang et al. 2016, 2017), except the snow scorpionflies *Boreus brumalis* Fitch and *Caurinus dectes* Russell, both of which have two equal mitochondrial derivatives (Dallai et al. 2003; Russell et al. 2013). In general, the larger mitochondrial derivative of mecopterans is circular in cross-section for its anterior portion, but assumes an asymmetric profile for most length of the tail (Dallai et al. 2003; Zhang and Hua 2017). The mitochondrial derivatives of *Terrobittacus*, however, are quite regular with a circular shape along the entire flagellum. This condition was also found in *Bittacus* (Shepardson et al. 2014) and can be considered a synapomorphic trait of Bittacidae.

In sum, the present study describes the ultrastructure of spermiogenesis and spermatozoa of *Terrobittacus* and provides some important characteristics for understanding the phylogeny of Bittacidae. However, the fine structure of the flagellar axoneme is not clear enough in some pictures, possibly owing to the imperfect fixation. The fixative method could be improved to preserve axoneme following Dallai and Afzelius (1990). The use of alternative materials (such as the epididymis, deferent ducts, and the spermatheca) may also work.

**Acknowledgements** We are grateful to Lu Liu for the assistance in specimen collection, Wei Du for the species identification, and Ke-Rang Huang and Xiao-Hua He for the technical assistance in transmission electron microscopy. We also thank two anonymous reviewers for their valuable comments and suggestions for the revision of the manuscript.

**Funding information** This research was funded by the National Natural Science Foundation of China (grant numbers 31672341 and 30970386).

## Compliance with ethical standards

**Conflict of interest** The authors declare that they have no conflict of interest.

**Ethical statement** This article does not contain any studies with vertebrate animals and human participants performed by any of the authors.

## References

- Baccetti B (1972) Insect sperm cells. *Adv Insect Physiol* 9:315–397. [https://doi.org/10.1016/S0065-2806\(08\)60279-9](https://doi.org/10.1016/S0065-2806(08)60279-9)
- Baccetti B (1998) Spermatozoa. In: Harrison FW, Locke M (eds) *Microscopic anatomy of invertebrates*, vol 11C. Insect. Wiley-Liss, New York, pp 843–894
- Beutel RG, Baum E (2008) A longstanding entomological problem finally solved? Head morphology of *Nannochorista* (Mecoptera, Insecta) and possible phylogenetic implications. *J Zool Syst Evol Res* 46: 346–367. <https://doi.org/10.1111/j.1439-0469.2008.00473.x>
- Bornemissza GF (1966) Observations on the hunting and mating behaviours of two species of scorpion flies (Bittacidae: Mecoptera). *Aust J Zool* 14:371–382. <https://doi.org/10.1071/ZO9660371>

- Breland OP, Gassner G, Riess WR, Biesile JJ (1966) Certain aspects of the centriole adjunct, spermiogenesis, and the mature sperm of insects. *Can J Genet Cytol* 8:759–773
- Byers GW, Thornhill R (1983) Biology of the Mecoptera. *Annu Rev Entomol* 28:203–228. <https://doi.org/10.1146/annurev.en.28.010183.001223>
- Cai L-J, Huang P-Y, Hua B-Z (2006) Two new Chinese *Bittacus* Latreille (Mecoptera: Bittacidae) from Micangshan Mountains. *Entomotaxonomia* 28:127–130
- Chapman RF (2013) Reproductive system: male. In: Simpson SJ, Douglas AE (eds) *The insects: structure and function*. Cambridge University Press, Cambridge, pp 290–291
- Chen J, Tan J-L, Hua B-Z (2013) Review of the Chinese *Bittacus* (Mecoptera: Bittacidae) with descriptions of three new species. *J Nat Hist* 47:1463–1480. <https://doi.org/10.1080/00222933.2012.763065>
- Cuquetto-Leite L, Dolder H, Oliveira PS, Espírito Santo NB, Lino-Neto J, Mancini KC (2017) Structural and ultrastructural characterization of the spermatozoa in *Pachycondyla striata* and *P. marginata*. *Insect Soc* 64:209–217. <https://doi.org/10.1007/s00040-016-0533-8>
- Dallai R (1979) An overview of atypical spermatozoa in insects. In: Fawcett DW, Bedford JM (eds) *The spermatozoon*. Urban and Schwarzenberg, Baltimore, pp 253–265
- Dallai R (2014) Overview on spermatogenesis and sperm structure of Hexapoda. *Arthropod Struct Dev* 43:257–290. <https://doi.org/10.1016/j.asd.2014.04.002>
- Dallai R, Afzelius BA (1990) Microtubular diversity in insect spermatozoa: results obtained with a new fixative. *J Struct Biol* 103:164–179. [https://doi.org/10.1016/1047-8477\(90\)90020-D](https://doi.org/10.1016/1047-8477(90)90020-D)
- Dallai R, Lupetti P, Frati F, Nardi F, Afzelius BA (2001) Sperm ultrastructure and spermiogenesis in the relic species *Tricholepidion gertschi* Wygodzinsky (Insecta, Zygentoma). *Tissue Cell* 33:596–605. <https://doi.org/10.1054/tice.2001.0214>
- Dallai R, Lupetti P, Afzelius BA, Frati F (2003) Sperm structure of Mecoptera and Siphonaptera (Insecta) and the phylogenetic position of *Boreus hyemalis*. *Zoomorphology* 122:211–220. <https://doi.org/10.1007/s00435-003-0087-y>
- Dallai R, Lupetti P, Mencarelli C (2006) Unusual axonemes of hexapod spermatozoa. *Int Rev Cytol* 254:45–99. [https://doi.org/10.1016/S0074-7696\(06\)54002-1](https://doi.org/10.1016/S0074-7696(06)54002-1)
- Dallai R, Mercati D, Carapelli A, Nardi F, Machida R, Sekiya K, Frati F (2011a) Sperm accessory microtubules suggest the placement of Diplura as the sister-group of Insecta s.s. *Arthropod Struct Dev* 40:77–92. <https://doi.org/10.1016/j.asd.2010.08.001>
- Dallai R, Mercati D, Gottardo M, Machida R, Mashimo Y, Beutel RG (2011b) The male reproductive system of *Zorotypus caudelli* Kamy (Zoraptera): sperm structure and spermiogenesis. *Arthropod Struct Dev* 40:531–547. <https://doi.org/10.1016/j.asd.2011.07.001>
- Dallai R, Gottardo M, Beutel RG (2016a) Structure and evolution of insect sperm: new interpretations in the age of phylogenomics. *Annu Rev Entomol* 61:1–23. <https://doi.org/10.1146/annurev-ento-010715-023555>
- Dallai R, Paoli F, Mercati D, Lupetti P (2016b) The centriole adjunct of insects: need to update the definition. *Tissue Cell* 48:104–113. <https://doi.org/10.1016/j.tice.2016.02.001>
- Dallai R, Mercati D, Lino-Neto J, Dias G, Folly C, Lupetti P (2019) The peculiar structure of the flagellar axoneme in Coccinellidae (Insecta–Coleoptera). *Arthropod Struct Dev* 49:50–61. <https://doi.org/10.1016/j.asd.2018.11.004>
- Dias G, Lino-Neto J, Mercati D, Dallai R (2015) The sperm ultrastructure and spermiogenesis of *Tribolium castaneum* (Coleoptera: Tenebrionidae) with evidence of cyst degeneration. *Micron* 73:21–27. <https://doi.org/10.1016/j.micron.2015.03.003>
- Friedrich F, Pohl H, Beckmann F, Beutel RG (2013) The head of *Merope tuber* (Meropeidae) and the phylogeny of Mecoptera (Hexapoda). *Arthropod Struct Dev* 42:69–88. <https://doi.org/10.1016/j.asd.2012.09.006>
- Gassner G, Breland OP, Biesile JJ (1972) The spermatozoa of the scorpionfly *Panorpa nuptialis*: a transmission electron microscope study. *Ann Entomol Soc Am* 65:1302–1309. <https://doi.org/10.1093/aesa/65.6.1302>
- Gottardo M, Mercati D, Dallai R (2012) The spermatogenesis and sperm structure of *Timema poppensis* (Insecta: Phasmatodea). *Zoomorphology* 131:209–223. <https://doi.org/10.1007/s00435-012-0158-z>
- Gottardo M, Dallai R, Mercati D, Hornschemeyer T, Beutel RG (2016) The evolution of insect sperm—an unusual character system in a megadiverse group. *J Zool Syst Evol Res* 54:237–256. <https://doi.org/10.1111/jzs.12136>
- Gottardo M, Persico V, Callaini G, Riparbelli MG (2018) The “transition zone” of the cilium-like regions in the *Drosophila* spermatocytes and the role of the C-tubule in axoneme assembly. *Exp Cell Res* 371:262–268. <https://doi.org/10.1016/j.yexcr.2018.08.020>
- Jamieson BGM, Dallai R, Afzelius BA (1999) *Insects: their spermatozoa and phylogeny*. Scientific Publishers, Enfield
- Karnovsky MJ (1964) A formaldehyde-glutaraldehyde fixative of high osmolality for use in electron microscopy. *J Cell Biol* 27:1A–149A
- Miao Y, Hua B-Z (2017) Cytogenetic comparison between *Terrobittacus implicatus* and *Bittacus planus* (Mecoptera: Bittacidae) with some phylogenetic implications. *Arthropod Syst Phyl* 75:175–183
- Nantel F, Monaco L, Foulkes NS, Masquillier D, LeMeur M, Henriksen K, Dierich A, Parvinen M, Sassone-Corsi P (1996) Spermiogenesis deficiency and germ-cell apoptosis in CREM-mutant mice. *Nature* 380:159–162. <https://doi.org/10.1038/380159a0>
- Nardi JB, Delgado JA, Collantes F, Miller LA, Bee CM, Kathirithamby J (2013) Sperm cells of a primitive strepsipteran. *Insects* 4:463–475. <https://doi.org/10.3390/insects4030463>
- Novais AM, Dias G, Lino-Neto J (2017) Testicular, spermatogenesis and sperm morphology in *Martarega bentoi* (Heteroptera: Notonectidae). *Arthropod Struct Dev* 46:635–643. <https://doi.org/10.1016/j.asd.2017.04.002>
- Penny ND (2006) A review of our knowledge of California Mecoptera. *Proc Calif Acad Sci* 57:365–372
- Phillips DM (1970) Insect sperm: their structure and morphogenesis. *J Cell Biol* 44:243–277
- Russell LK, Dallai R, Gottardo M, Beutel RG (2013) The sperm ultrastructure of *Caurinus dectes* Russell (Mecoptera: Boreidae) and its phylogenetic implications. *Tissue Cell* 45:397–401. <https://doi.org/10.1016/j.tice.2013.07.001>
- Santos ABR, Lino-Neto J (2018) Sperm morphology of predatory pirate bugs *Amphiareus constrictus* and *Blaptostethus pallescens* (Heteroptera: Anthocoridae) with phylogenetic inferences. *Micron* 105:18–23. <https://doi.org/10.1016/j.micron.2017.11.004>
- Shepardson SP, Humphries BA, Pelkki KL, Stanton DJ (2014) Spermatozoon ultrastructure of hangingflies, *Bittacus strigosus* and *Bittacus stigmaterus*. *J Insect Sci* 14:10. <https://doi.org/10.1093/jis/14.1.10>
- Tan J-L, Hua B-Z (2008) Structure of raptorial legs in *Bittacus* (Mecoptera : Bittacidae). *Acta Entomol Sin* 51:745–752
- Tan J-L, Hua B-Z (2009) *Terrobittacus*, a new genus of the Chinese Bittacidae (Mecoptera) with descriptions of two new species. *J Nat Hist* 43:2937–2954. <https://doi.org/10.1080/00222930903359628>
- Whiting MF (2002) Mecoptera is paraphyletic: multiple genes and phylogeny of Mecoptera and Siphonaptera. *Zool Scr* 31:93–104. <https://doi.org/10.1046/j.0300-3256.2001.00095.x>
- Willmann R (1987) The phylogenetic system of the Mecoptera. *Syst Entomol* 12:519–524. <https://doi.org/10.1111/j.1365-3113.1987.tb00222.x>
- Willmann R (1989) Evolution und phylogenetisches system der Mecoptera (Insecta: Holometabola). *Abh Senckenb Natforsch Ges* 544:1–153

- Zhang B-B, Hua B-Z (2014) Sperm ultrastructure of *Panorpodes kuandianensis* (Mecoptera: Panorpididae). *Microsc Res Tech* 77: 394–400. <https://doi.org/10.1002/jemt.22357>
- Zhang B-B, Hua B-Z (2017) Spermatogenesis and sperm structure of *Neopanorpa lui* and *Neopanorpa lipingensis* (Mecoptera: Panorpididae) with phylogenetic considerations. *Arthropod Syst Phyl* 75:373–386
- Zhang B-B, Lyu Q-H, Hua B-Z (2016) Male reproductive system and sperm ultrastructure of *Furcatopanorpa longihypovalva* (Hua and Cai, 2009) (Mecoptera: Panorpididae) and its phylogenetic implication. *Zool Anz* 264:41–46. <https://doi.org/10.1016/j.jcz.2016.07.004>
- Zhang B-B, Xie S, Hua B-Z (2017) Spermatogenesis and sperm ultrastructure of *Panorpa liui* Hua (Mecoptera: Panorpididae). *Acta Entomol Sin* 60:389–400. <https://doi.org/10.16380/j.kcxb.2017.04.004>
- Zizzari ZV, Lupetti P, Mencarelli C, Dallai R (2008) Sperm ultrastructure and spermiogenesis of Coniopterygidae (Neuroptera, Insecta). *Arthropod Struct Dev* 37:410–417. <https://doi.org/10.1016/j.asd.2008.03.001>

**Publisher's note** Springer Nature remains neutral with regard to jurisdictional claims in published maps and institutional affiliations.